Pramāṇa – J. Phys., Vol. 34, No. 4, April 1990, pp. 333–345. © Printed in India.

Evaluation of downstream-mixing scheme for 9·4-μm CO_2 gasdynamic laser

P CHAKRAVARTY, N M REDDY and K P J REDDY
Department of Aerospace Engineering, Indian Institute of Science, Bangalore 560012, India

MS received 9 August 1989; revised 4 January 1990

Abstract. A theoretical analysis of a downstream-mixing 16-μm CO_2 gasdynamic laser revealed the possibility of utilizing the downstream-mixing scheme for the generation of 9·4-μm radiation using a CO_2 gasdynamic laser. The flow-field has been analyzed using complete two-dimensional, unsteady laminar form of Navier-Stokes equations coupled with the finite rate vibrational kinetic equations. The analysis showed that integrated small-signal gain of 11·5 m^{-1} for Lorentzian broadening and 4·8 m^{-1} considering Voigt function can be obtained for N_2 reservoir temperature of 2000°K and velocity ratio 1:1 between the CO_2 and N_2 mixing streams. These results (presented in graphs) clearly highlight the large potential of downstream-mixing CO_2 gasdynamic laser for 9·4-μm laser generation.

Keywords. Downstream-mixing gasdynamic laser; small-signal gain.

PACS Nos 42·55; 51·70; 42·80

1. Introduction

Since the first proposal for the generation of 16-μm laser beam in CO_2 gasdynamic laser (GDL), which can effectively be used for the laser isotope separation of uranium, there has been a lot of interest in the study of this system. Majority of publications in this field are theoretical and the results are very encouraging. The laser action at 16-μm is achieved by creating the population inversion between (02^00) and (01^10) levels of CO_2 molecule. One of the important assumptions in these studies is that an intense, saturating laser pulse of 9·4-μm is injected into the laser mixture downstream of the nozzle throat to induce transition of molecules from (00^01) level to (02^00) level such that, for a short time a net population inversion is created between (02^00) and (01^10) levels which results in 16-μm laser generation. However, this puts serious constraints on to the system experimentally in terms of choosing 9·4-μm laser pulse of right power, shape and duration. Thus, because of the complex optics involved in this technique, the system becomes very complicated and the overall efficiency goes down.

An effective way of evading this problem is to generate 16-μm beam through cascading process where the population inversion for this transition is achieved by generating a 9·4-μm laser internally from the transition between (00^01) and (02^00) levels of CO_2 molecule. Such a scheme has been investigated theoretically for a premixed cascading 16-μm CO_2 GDL (Saito *et al* 1982), and has been found to be able to render better performance than the above mentioned earlier system. A possible approach for further improvement of performance is the use of downstream-mixing

scheme in cascaded 16-μm CO_2 GDL. This downstream-mixing scheme is already well known for high performance at 10·6-μm for CO_2 GDLs (Cassady 1980; Murthy 1975; Losev 1981 and Anderson 1976). Further, this approach for the 9·4-μm pulse injected 16-μm CO_2 GDL, has also been proved analytically to be able to produce very high gain values for 16-μm (Chakravarty and Reddy 1986). However, to employ this scheme in actual practice for cascading 16-μm CO_2 GDL requires the generation of 9·4-μm lasing inside a CO_2-N_2 downstream-mixing GDL. This process is quite complex physically. In actual mixing region there is rise in static temperature due to total temperature recovery and consequent increase in the lower laser level (02^00) population. Thus this rise can reduce the population inversion between (00^01) and (02^00) laser levels and in turn degrade the laser action. Moreover, throughout the finite mixing region of the flow, vibrational deactivation can also decrease the lasing action. Furthermore, in actual practice it takes a finite amount of time for mixing, and hence for the molecular collision to occur, before N_2 can pump the CO_2 molecules to higher levels. Thus due to the lapse of this finite amount of time in the process of getting vibrationally excited CO_2 molecules, the 9·4-μm laser action may get affected badly due to the temperature rise. This may in turn jeopardize the 16-μm generation through cascading process. Therefore, before attempting to study such a cascade operation it is essential to evaluate the potential of 9·4-μm generation from a CO_2 downstream-mixing GDL. Also, its properties and characteristics along and across the flow-field are required to be known. In this connection, no detailed study for 9·4-μm has been reported in the literature except for some feasibility studies indicating only the possibility of generation of 9·4-μm lasing for generating 16-μm, theoretically using one-dimensional approaches from premixed CO_2 GDLs by Saito *et al* (1982), Biryukov *et al* (1981), (1984) and also from CO_2 electric discharge lasers by Zaroslov *et al* (1982), and experimentally from a CO_2 after mixing type electric discharge GDL by Wexler *et al* (1977) and Wexler and Waynant (1979). Also, no work has been reported on CO_2 downstream-mixing GDL for generation of 9·4-μm lasing action when this system is well proven to have high performance for other lasing wavelengths of CO_2 i.e., 10·6-μm and 16-μm, as mentioned above. Therefore, it is in this spirit that a study of the 9·4-μm generation from CO_2 downstream-mixing GDL has been carried out and the results of this study are presented in this paper.

The flow-field of a 9·4-μm CO_2 downstream-mixing GDL has been analyzed, using a model utilizing the complete two-dimensional, unsteady, laminar Navier-Stokes equations, fully coupled with the finite rate vibrational kinetic equations. This analysis emphasizes the fluid dynamic and kinetic aspects of the mixing flow taking into consideration the detailed collisional deactivation rate processes in the mixing region. Further, this work contributes to the understanding of 9·4-μm CO_2 downstream-mixing GDL largely by giving a detailed analysis of the various properties of it along the flow-field, and also the effect of variation of different flow-field parameters on the 9·4-μm small-signal gain. The results of numerical study clearly show for the first time the high potential of "downstream-mixing" scheme for 9·4-μm CO_2 GDL and thereby highlighting, that, a 9·4-μm CO_2 laser of such type can further be used for the generation of a 16-μm laser through the cascade process.

2. Simulation model and governing equations

The simulation model used for the present analysis is explained in detail by

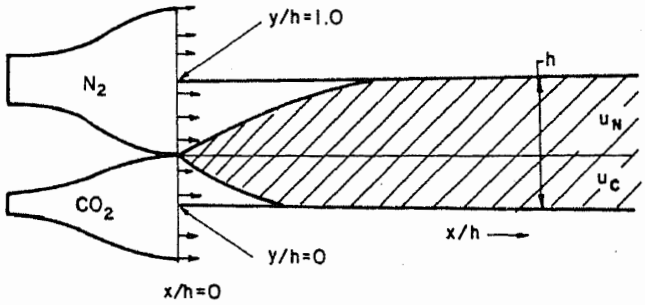

Figure 1a. Schematic diagram of a downstream-mixing gasdynamic laser.

Chakravarty and Reddy (1986) and Chakravarty (1989). Figure 1(a) illustrates the physical setup of the downstream-mixing GDL used for the present analysis. The two nozzles shown are assumed to be only part of a bank of multiple nozzles characteristics of GDLs; thereby the two centrelines are lines of symmetry. The region of interest for the present analysis starts from the nozzle exits, extends downstream and remains confined between two centrelines. This region for the sake of simplicity is referred as duct. A supersonic stream of vibrationally excited pure N_2 is mixed tangentially with a supersonic stream of cold CO_2 at the nozzle exits. Due to mixing through molecular collisions, vibrational energy is transferred from N_2 to cold CO_2. The flow-field has been assumed to be laminar (by keeping the Reynolds number low) and two-dimensional in spatial directions x and y as shown in Figure 1(a).

In the present analysis both the streams are considered to be compressible and viscous, with varying viscosity, thermal conductivity and diffusivity. They are also non-radiating and have non-equilibrium vibrational energy exchange between themselves. Thus the basic set of equations are unsteady, two-dimensional form of laminar Navier-Stokes equations, augmented with appropriate species continuity, global continuity, energy, state equation and the vibrational relaxation equations, which can be expressed as:

Continuity

$$\frac{\partial \rho}{\partial t} + \frac{\partial}{\partial x}(\rho u) + \frac{\partial}{\partial y}(\rho v) = 0. \tag{1}$$

Species continuity

$$\frac{\partial}{\partial t}(\rho c_i) + \frac{\partial}{\partial x}(\rho u c_i) + \frac{\partial}{\partial y}(\rho v c_i) + \frac{\partial}{\partial x}(\rho_i u_i) + \frac{\partial}{\partial y}(\rho_i v_i) = 0. \tag{2}$$

x-momentum

$$\frac{\partial}{\partial t}(\rho u) + \frac{\partial}{\partial x}\left[\rho uu + p + \frac{2}{3}\mu\left(\frac{\partial u}{\partial x} + \frac{\partial v}{\partial y}\right) - 2\mu\frac{\partial u}{\partial x}\right] + \frac{\partial}{\partial y}\left[\rho uv - \mu\left(\frac{\partial u}{\partial y} + \frac{\partial v}{\partial x}\right)\right] = 0. \tag{3}$$

y-momentum

$$\frac{\partial}{\partial t}(\rho v)+\frac{\partial}{\partial y}\left[\rho vv+p+\frac{2}{3}\mu\left(\frac{\partial u}{\partial x}+\frac{\partial v}{\partial y}\right)-2\mu\frac{\partial v}{\partial y}\right]$$
$$+\frac{\partial}{\partial x}\left[\rho uv-\mu\left(\frac{\partial u}{\partial y}+\frac{\partial v}{\partial x}\right)\right]=0. \tag{4}$$

Energy

$$\frac{\partial}{\partial t}(\rho h)+\frac{\partial}{\partial x}(\rho uh)+\frac{\partial}{\partial y}(\rho vh)$$
$$=\frac{\partial}{\partial x}\left(k\frac{\partial T}{\partial x}\right)+\frac{\partial}{\partial y}\left(k\frac{\partial T}{\partial y}\right)-\frac{\partial}{\partial x}\left(\sum_i \rho_i u_i h_i\right)$$
$$-\frac{\partial}{\partial y}\left(\sum_i \rho_i v_i h_i\right)+\frac{\partial p}{\partial t}+u\frac{\partial p}{\partial x}+v\frac{\partial p}{\partial y}$$
$$+\mu\left[2\left[\left(\frac{\partial u}{\partial x}\right)^2+\left(\frac{\partial v}{\partial y}\right)^2\right]+\left(\frac{\partial v}{\partial x}+\frac{\partial u}{\partial y}\right)^2-\frac{2}{3}\left(\frac{\partial u}{\partial x}+\frac{\partial v}{\partial y}\right)^2\right]. \tag{5}$$

State

$$p=\rho RT. \tag{6}$$

In addition to these equations, as explained earlier, a set of vibrational relaxation equations are added to find out the vibrational energies of the appropriate levels of CO_2, taking into consideration the non-equilibrium vibrational energy exchange between the two mixing streams. The present system being a downstream-mixing GDL, the pumping rate of the (001) level of CO_2 by N_2 is the controlling factor in the evaluation of laser gain as the flow moves downstream of the nozzle exits. Hence, the detailed vibrational kinetic model by Munjee (1972), where the ν_3 mode of CO_2 is kept separate from N_2, has been considered for the present analysis (figure 1(b)). In this model due to strong Fermi resonance between the ν_1 and ν_2 modes of CO_2, they are combined together as ν_{12}, with associated vibrational energies and

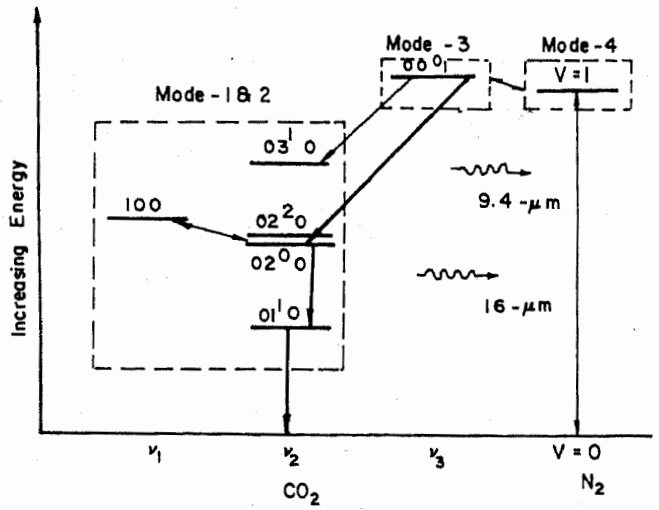

Figure 1b. Schematic diagram of vibrational energy levels of CO_2 and N_2 molecules.

temperatures as $e_{12} = e_1 + 2e_2$ and $T_{12} = T_1 = T_2$ respectively. However, the present system being a flowing system where, the vibrational energy in a given mode changes not only due to collisions but also due to convection and viscous diffusion, the time rates of net energy transfer into or out of these modes derived using the above model can be expressed as

$$\frac{\partial}{\partial t}(\rho e_{\text{vib}_{12}}) = -\frac{\partial}{\partial x}(\rho e_{\text{vib}_{12}} u) - \frac{\partial}{\partial y}(\rho e_{\text{vib}_{12}} v) + \frac{\partial}{\partial x}\left(\rho D_{12}\frac{\partial c_{\text{CO}_2}}{\partial x} e_{12}\right) + \frac{\partial}{\partial y}\left(\rho D_{12}\frac{\partial c_{\text{CO}_2}}{\partial y} e_{12}\right) + \rho_{\text{CO}_2}\dot{w}_{12} \tag{7}$$

$$\frac{\partial}{\partial t}(\rho e_{\text{vib}_3}) = -\frac{\partial}{\partial x}(\rho e_{\text{vib}_3} u) - \frac{\partial}{\partial y}(\rho e_{\text{vib}_3} v) + \frac{\partial}{\partial x}\left(\rho D_{12}\frac{\partial c_{\text{CO}_2}}{\partial x} e_3\right) + \frac{\partial}{\partial y}\left(\rho D_{12}\frac{\partial c_{\text{CO}_2}}{\partial y} e_3\right) + \rho_{\text{CO}_2}\dot{w}_3 \tag{8}$$

$$\frac{\partial}{\partial t}(\rho e_{\text{vib}_4}) = -\frac{\partial}{\partial x}(\rho e_{\text{vib}_4} u) - \frac{\partial}{\partial y}(\rho e_{\text{vib}_4} v) + \frac{\partial}{\partial x}\left(\rho D_{12}\frac{\partial c_{\text{N}_2}}{\partial x} e_4\right) + \frac{\partial}{\partial y}\left(\rho D_{12}\frac{\partial c_{\text{N}_2}}{\partial y} e_4\right) + \rho_{\text{N}_2}\dot{w}_4. \tag{9}$$

Here, u, v are the velocities of the mixture relative to the laboratory or fixed frame, u_i, v_i are the diffusion velocities of species i relative to the mass-motion of the mixture, ρ_i is the density of species i, ρ and p are the static density and static pressure of the mixture, T is the static temperature, c_i is the mass-fraction of species i, h_i is the static enthalpy of species i, h is the static enthalpy of the mixture, μ is the dynamic viscosity coefficient of the mixture, k is the coefficient of thermal conductivity of the mixture, R is the specific gas constant of the mixture, D_{12} is the binary diffusion coefficient, e_{12}, e_3 are the vibrational energies per unit mass of CO_2 in mode-12 and mode-3 respectively, e_4 is the vibrational energy in mode-4 per unit mass of N_2, $e_{\text{vib}_{12}}$, e_{vib_3}, e_{vib_4} are the vibrational energies per unit mass of the mixture in modes 12, 3 and 4 respectively, $\dot{w}_{12}, \dot{w}_3, \dot{w}_4$ are the time rates of net energy transfer into our out of modes 12, 3 and 4 respectively from Munjee's model.

The above equations are nondimensionalized and solved numerically following the method given by Chakravarty *et al* (1986), (1987) and Chakravarty (1989), using an explicit, time-dependent, second-order accurate, finite-difference, computer code, based on the predictor-corrector approach of MacCormack to find out the steady-state values of flow-field variables. The flow-field properties are calculated as functions of x (in the flow direction) and y (normal to the flow direction i.e., the laser beam direction) as shown in figure 1(a). These steady-state values are further used to calculate the population inversion between (00^01) and (02^00) levels of CO_2 (Fig. 1(b)) and in turn the 9·4-μm small-signal gain. The small-signal gain expression for $P(14)$ line of (00^01)–(02^00) transition considering only Lorentzian broadening with rotational correction can be expressed as:

$$G_{L9\cdot4} = \frac{\lambda^2}{4\pi\tau_{12}Z}\left(\frac{32\cdot546842}{T}\right)(\text{N}_{00^01} - \text{N}_{02^00})\exp(-117\cdot84201/T) \tag{10}$$

where $\lambda = 9{\cdot}4$-μm is the wavelength of the laser, $\tau_{12} = 5{\cdot}0$ s is the radiative life time (Manuccia *et al* 1976), Z is the molecular collision frequency, N_i is the population of the ith level.

However, for a gas which is expanded from high stagnation pressure to very low static pressures at the optical cavity, as in a GDL especially of the kind simulated in the present analysis, consideration of both Lorentz and Doppler line-broadening mechanisms become important for the evaluation of line shape function. Therefore, in this investigation the 9·4-μm small-signal gain values have been recalculated using Voigt function $H(a, 0)$, which combines the effect of both the line-broadening mechanisms. With the above modification the 9·4-μm small-signal gain expression with rotational correction is:

$$G_{V9\cdot4} = \frac{\lambda^2}{8\pi\tau_{12}}\left(\frac{32{\cdot}546842}{T}\right)(N_{00^01} - N_{02^00})\exp\left(\frac{-117{\cdot}84201}{T}\right) \times \left(\frac{\ln 2}{\pi}\right)^{1/2}\frac{H(a,0)}{\Delta\nu_D}. \tag{11}$$

Where $\Delta\nu_D$ is the Doppler half-width. The method of evaluation of Voigt function $H(a, 0)$, is given in detail in Chakravarty (1989) and also in Gross and Bott (1976).

3. Results and discussion

The initial conditions used for the present analysis are $T_{o_{N_2}} = 2000°K$, $p_{o_{N_2}} = 2 \times 10^6$ N/m^2, reference temperature at the nozzle exists = 141·94°K, reference pressure at the nozzle exits = 199·5 N/m^2, Mach number = 8·09 and velocity ratio between the CO_2 and N_2 streams $u_C : u_N = 1:1$. The N_2 vibrational temperature is assumed to be frozen during the nozzle expansion process, so that, $T_{vib_{N_2}} = T_{o_{N_2}} = 2000°K$. The CO_2 vibrational modes are assumed to be in equilibrium with the translational and rotational modes during the nozzle expansion process, hence $T_{vib_{CO_2}}$ = reference static temperature = 141·94°K. During the computation, grid points in the transverse direction have been assumed such that the CO_2 stream extends from $y/h = 0{\cdot}0$ to $y/h = 0{\cdot}35$, and there is only N_2 stream beyond this range.

In the present analysis though the numerical method used to solve the flow-field equations is a time dependent method, all results presented in this section are the final steady-state values. The intermediate transients are of no particular interest and are not given here. In the figures the parameters with subscript R are the reference quantities used for non-dimensionalising the variables in the governing equations. These reference quantities are the N_2 stream values at the nozzle exit.

The steady-state transverse velocity distribution profiles of the system shown in figure 1(a) having velocity ratio $u_C : u_N = 1:1$ are shown in figure 2. It has already been established from our earlier investigation (Chakravarty and Reddy 1986 and Chakravarty *et al* 1987), that velocity ratio 1:1 leads to best possible gain values for 16-μm. In this study since the system configuration and initial conditions are kept same as in the previous studies, the velocity ratio has been chosen as 1:1. It can be observed here that there is no velocity discontinuity even till far downstream at $x/h = 200$. This leads to many advantages as will be elaborated in the following discussion. Further, figure 3 presents the transverse mixture-density distribution

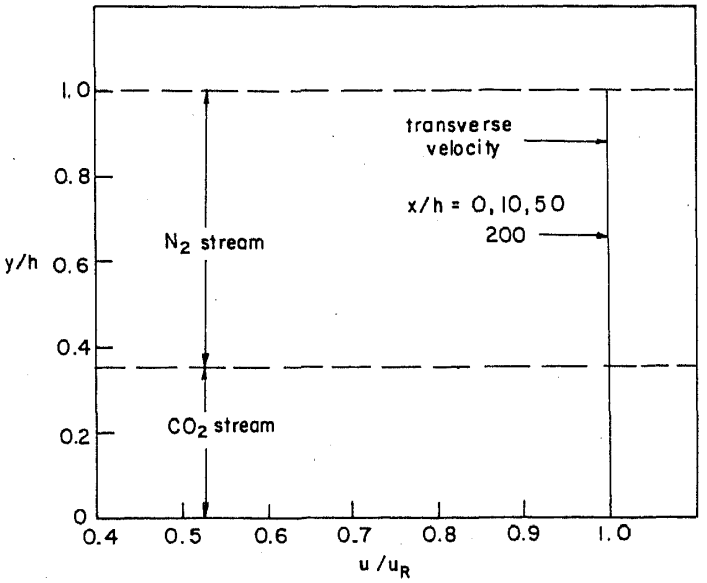

Figure 2. Transverse velocity distribution profiles at various axial locations in the cavity.

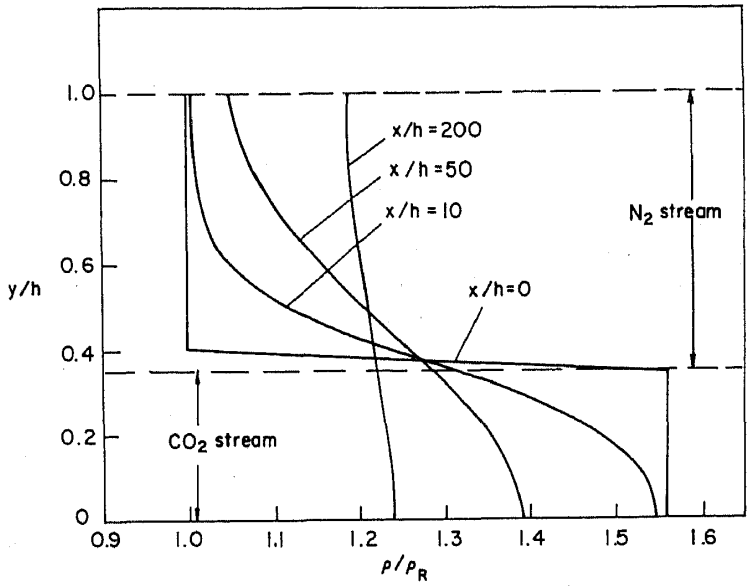

Figure 3. Transverse mixture-density distribution profiles at various axial locations in the cavity.

profiles at various axial locations. The large initial density gradients near the inlet become almost uniform by $x/h = 200$. The peak value of $\Delta\rho/\rho$ at $x/h = 200$ is only 5·2%. Such uniform mixed region with low values of density distributions are necessary for good optical quality of the laser beam.

The vibrational energy profiles of the CO_2-N_2 system under consideration are presented in figures 4, 5 and 6. The vibrational energy transfer process is a complex phenomenon. Furthermore, the vibrational energy of the molecules inside a moving fluid element in the mixing flow-field is changed by convection and diffusion of vibrational species across the fluid element boundaries and by vibrational energy exchange with other molecules that are inside the fluid element as well as with those

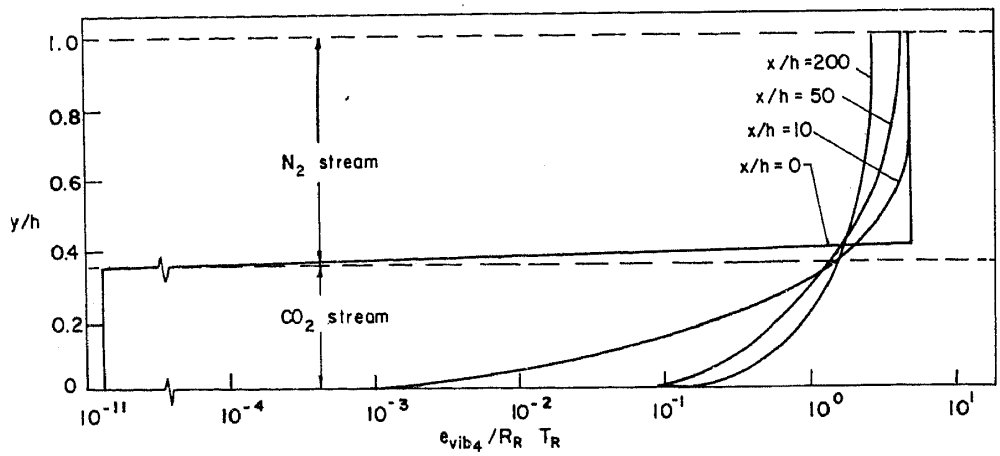

Figure 4. Transverse profiles of vibrational energy in mode-4 at various axial locations in the cavity.

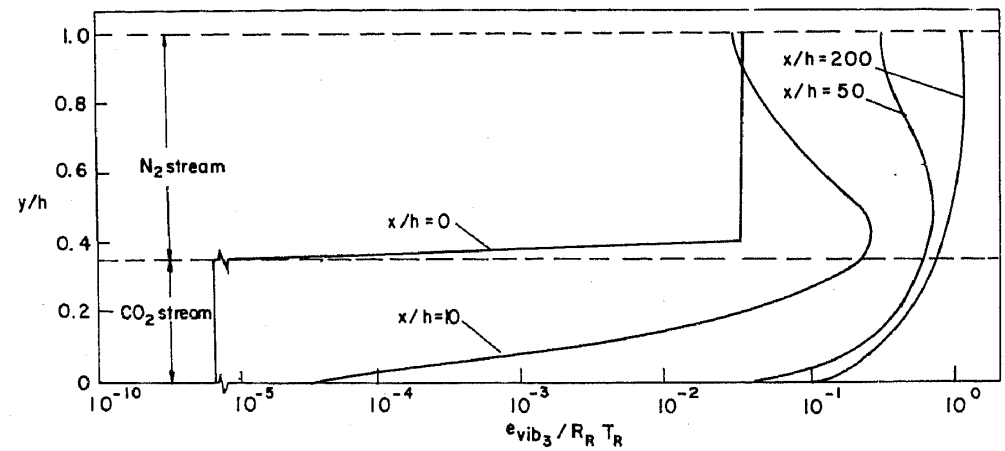

Figure 5. Transverse profiles of vibrational energy in mode-3 at various axial locations in the cavity.

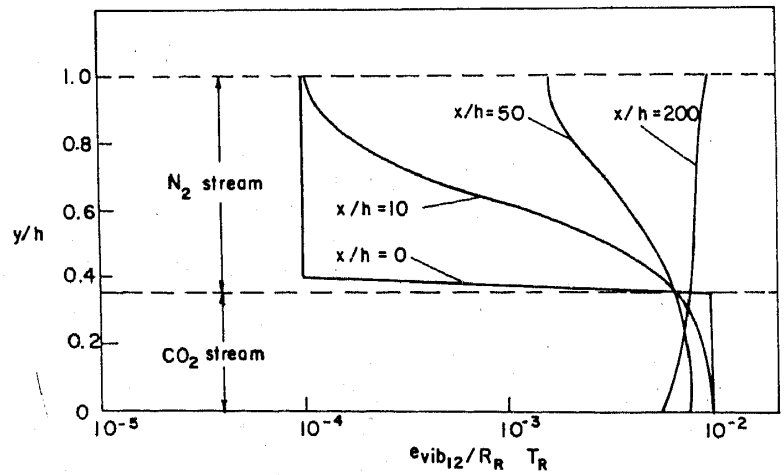

Figure 6. Transverse profiles of vibrational energy in mode-12 at various axial locations in the cavity.

that diffuse across the boundaries. It is the result of these complex processes that are reflected in the vibrational energy profiles.

Figure 4 shows the profiles of vibrational energy in mode-4. The energy e_{vib_4} increases from a very low value at $y/h = 0$ and $x/h = 10$, to an appreciably higher value at $y/h = 0$ and $x/h = 200$. This is due to the presence of vibrationally excited N_2 in the CO_2 stream as a result of diffusion from the N_2 stream. On the other hand, due to the existence of N_2 in the upper stream, e_{vib_4} does not change appreciably even far downstream at $x/h = 200$, a fact that is reflected in the upper portion of the curve at $y/h = 1{\cdot}0$. An interesting feature of the initial steady-state distribution profile in this figure is that, the e_{vib_4} is negligibly small at $x/h = 0$, from $y/h = 0$ to $0{\cdot}35$. This is attributed to the fact that there are practically no vibrationally excited N_2 molecules present in the CO_2 stream at the nozzle exits. This means that, in the process of attainment of steady-state at $x/h = 0$, during the time elapsed, even if a handful of excited N_2 molecules have diffused into the CO_2 stream, they have quickly transferred their energy to CO_2 molecules due to near resonant energy transfer collision. As a result, there is no excited N_2 molecule present in that region to contribute for e_{vib_4}. On the other hand, e_{vib_4} is quite large in the N_2 stream region i.e., $y/h = 0{\cdot}4$ to $1{\cdot}0$ at $x/h = 0$, due to the presence of large number of excited N_2 molecules.

The profiles of vibrational energy in mode-3 are presented in figure 5. These profiles of e_{vib_3} are the direct measure of population in the (001) level of CO_2, which gives rise to 9·4-μm laser emission. Thus, higher e_{vib_3} means higher gain for 9·4-μm transition. Here at $x/h = 0$, up to $y/h = 0{\cdot}35$ the e_{vib_3} is very small, which implies that in a downstream-mixing GDL at the exit of the nozzle, CO_2 is very cold and hence mode-3 is practically empty. However, at $y/h = 0{\cdot}4$ onwards (at the same $x/h = 0$) there is large increase in e_{vib_3}. By similar reasoning as given for figure 4 in the process of attainment of steady-state at $x/h = 0$, during the time elapsed a few of the CO_2 molecules diffuse into the N_2 stream and give rise to increase in e_{vib_3}. There is a large increase in e_{vib_3} far downstream due to mixing at $x/h = 200$ and $y/h = 0$. Also, from $y/h = 0{\cdot}4$ and upwards, distribution of e_{vib_3} is uniform. This is a very important feature, since it leads to almost uniform small-signal gain profiles as will be explained in the following discussion.

Figure 6 is a representation of vibrational energy in mode-12. This mode due to its lower energy level is in near equilibrium with the translational mode, and it reflects the changes in the static temperature T. The change in the $e_{vib_{12}}$ in the region $y/h = 0$ to $0{\cdot}35$ is negligible for various x/h values, which implies that, the change in static temperature of the system is negligible even far downstream at $x/h = 200$, compared to that at $x/h = 0$. This fact will be elaborated later during the discussion of figures 7 and 8. However, the little decrease of $e_{vib_{12}}$ in this region as seen in figure 6 can be attributed to the following reasons. The diffusion of $e_{vib_{12}}$ to other parts of the stream is one reason, due to which there is appreciable increase in $e_{vib_{12}}$ above $y/h = 0{\cdot}35$ at $x/h = 200$. Also collisionally deactivated CO_2 molecules to the ground state have a higher probability of being pumped to the (001) level because of the increased amount of vibrationally excited N_2 that has diffused into the CO_2 stream. In the N_2 stream region, between $y/h = 0{\cdot}35$ to $y/h = 1{\cdot}0$, from $x/h = 0$ to 10, there are very few CO_2 molecules and hence $e_{vib_{12}}$ is low. This $e_{vib_{12}}$ in this region increases at $x/h = 200$, as explained earlier, due to mixing.

All these observations are further borne out by the plots of static temperature T and the vibrational temperatures T_{12}, T_3 and T_4 for the modes 12, 3 and 4 given in

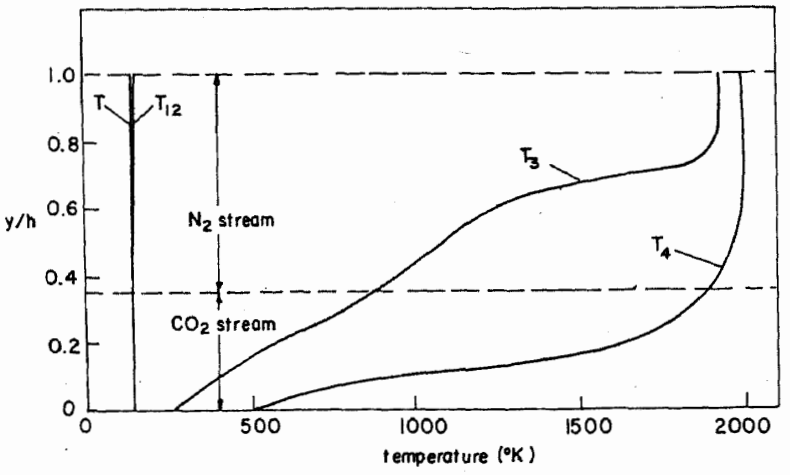

Figure 7. Transverse profiles of static temperature (T) and vibrational temperatures of the modes (12), (3) and (4) at $x/h = 10$.

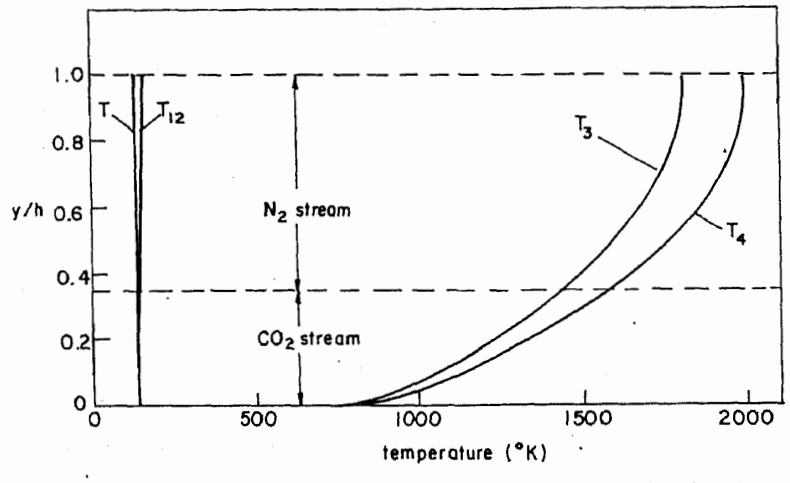

Figure 8. Transverse profiles of static temperature (T) and vibrational temperatures of the modes (12), (3) and (4) at $x/h = 200$.

figures 7 and 8. It can be seen, that in support of earlier discussion on figure 6, the static temperature T remains almost constant from $x/h = 10$ to far downstream $x/h = 200$ as shown in figures 7 and 8. This is due to the reason that the effect of viscous dissipation in increasing the static temperature has been completely eliminated because there is no velocity discontinuity between the two streams as shown in figure 2. The mixing of two streams in this case is only by diffusion. Hence there is no appreciable rise in static temperature. It can be noticed that the temperature T_{12} is slightly different from the static temperature above $y/h = 0{\cdot}35$ at $x/h = 200$. This supports the earlier explanation that some of the CO_2 molecules that diffuse into the N_2 streams are vibrationally excited not only into mode 3 but also into mode 12. Further, at $x/h = 10$ in figure 7, the temperature T_3 and T_4 are far apart indicating that the resonant transfer of vibrational energy from N_2 to CO_2 has not occurred to any significant extent. However, at $x/h = 200$ in figure 8, the T_3 and T_4 temperature profiles lie very close to each other indicating that the pumping of CO_2 molecules by N_2 is nearly complete. Thus these profiles show that the (001) level of CO_2 and ($V = 1$) level of

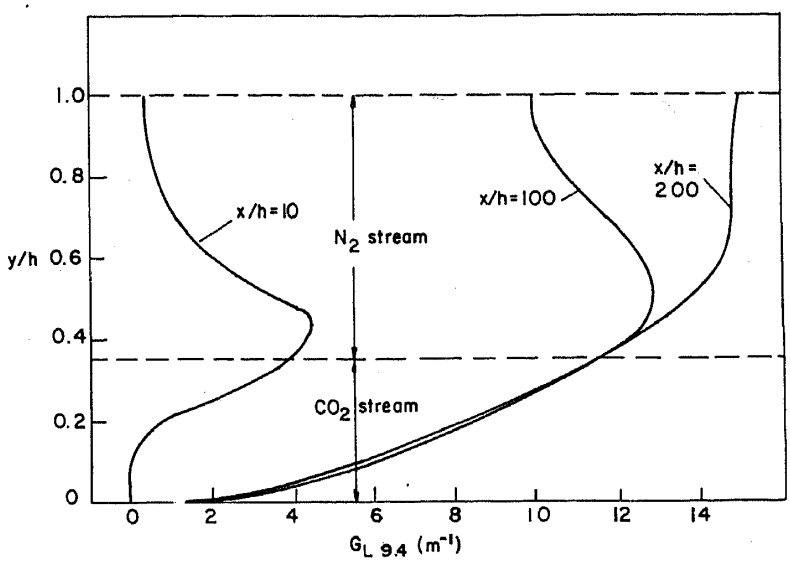

Figure 9. Transverse profiles of local small-signal gain at various axial locations in the cavity.

N_2 equilibrate while mode 12 closely follows the translational mode indicating a population inversion between the two laser levels namely ($00^0 1$) and ($02^0 0$) especially at far downstream.

The testimony of this population inversion is finally brought out in the local small-signal gain $G_{L9\cdot4}$ profiles as shown in figure 9. These plots are obtained using (10). The strong gradients in $G_{L9\cdot4}$ near the inlet are attenuated as the two streams mix farther downstream. These strong gradients near the initial axial locations appear in the good mixing region i.e., in the middle of the flow, between $y/h = 0{\cdot}4$ to $0{\cdot}6$, due to the availability of more number of excited CO_2 molecules, which contribute to the gain. However, in support of our earlier observations (figures 3 and 5), more uniform gain region evolves only at far downstream due to creation of homogeneously mixed total flow-field, as shown by the upper portion of the curve at $x/h = 200$, reflecting the point that far downstream, the flow gradually tends towards that of a conventional 9·4-μm GDL. The highest value of local small-signal gain obtained from the present analysis, at $x/h = 200$ is $14{\cdot}9\,m^{-1}$. This value of $G_{L9\cdot4}$ at N_2 reservoir temperature 2000°K is even when the detailed collisional deactivation rate processes in the mixing zone are considered in the analysis. Further, from the previous experience of the authors for the 9·4-μm induced 16-μm CO_2-N_2 downstream mixing GDL (Chakravarty *et al* 1986, 1987), it is expected that the above mentioned value of $G_{L9\cdot4}$ for the present CO_2 downstream-mixing GDL is higher than a conventional CO_2 GDL with the same reservoir temperature of 2000°K. However, no quantitative comparison of this result can be made at present due to lack of data.

Figure 10 presents the variation of integrated gain with distance along the flow. These plots are obtained by integrating the local small-signal gain profiles individually, along y/h, at particular x-location. Hence, such a plot represents the average small-signal gain axially, as a result it can express the overall laser quality of the mixing flow. The upper plot (a) in this figure corresponds to figure 9 i.e., the integrated gain obtained from the local small-signal gain $G_{L9\cdot4}$ distribution, computed using eqn. (10). Whereas, the lower plot (b) is corresponding to the local small-signal gain $G_{V9\cdot4}$ distribution, obtained using Eqn. (11), i.e., considering the effect of Voigt

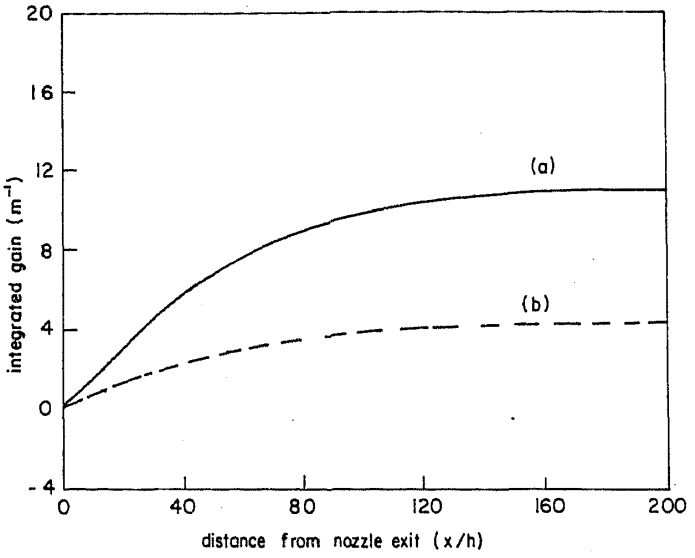

Figure 10. Variation of average small-signal gain (integrated gain) along the flow for (a) Lorentzian broadening and (b) Lorentzian-Doppler broadening.

function. The highest value of integrated gain for the upper and lower plot at $x/h = 200$ is $11{\cdot}5\,m^{-1}$ and $4{\cdot}8\,m^{-1}$ respectively. Although, there is a definite decrease in the gain results as shown by plot (b) compared to plot (a), however, they are still large and also due to the reasons mentioned earlier these results are definitely more accurate than the results of plot (a) computed assuming pure Lorentzian broadening. Also, in support of our earlier obervations (figures 3 and 5), the peak integrated gain tends to become constant downstream of $x/h = 140$, this behaviour is beneficial to good laser quality. Another important inference is that from station $x/h = 140$ onwards enough population inversion is expected to buildup upon resuming the 9·4-μm lasing to give rise to a 16-μm laser action.

4. Conclusions

The theoretical analysis of the 9·4-μm CO_2 downstream-mixing GDL is presented in detail. From the analysis it is shown that such a GDL can easily produce the power levels required for industrial applications with 9·4-μm radiation. It has been shown that the peak integrated gain value of $11{\cdot}5\,m^{-1}$ considering Lorentzian broadening is achievable on the $P(14)$ line of the (001)–(020) transition. However, this gain value reduces to $4{\cdot}8\,m^{-1}$ when Voigt function is considered for line shape, which is more realistic for the experimental set up simulated in the present investigation. The study of variation of peak gain along the downstream of the nozzle has shown that the gain remains constant after reaching a maximum value. The gain values reported here are higher than the conventional 9·4-μm CO_2 GDL gain values. In addition, these high values of 9·4-μm gain are clear indication of the possibility of internal generation of 9·4-μm lasing action which in turn may generate 16-μm lasing through cascading process.

It is recommended to have 1:1 velocity ratio between the CO_2 and N_2 mixing streams to reduce the viscous heating and hence the total temperature recovery in

the mixing region. Further, the laminar mixing, though slow, is found to be very efficient as it gave rise to uniform mixed regions with homogeneous density distribution at large distances.

Acknowledgement

One of the authors (PC) gratefully acknowledges the financial assistance provided by the Council of Scientific and Industrial Research, New Delhi by awarding him the Senior Research Fellowship in Engineering.

References

Anderson J D Jr 1976 *Gasdynamic lasers: An introduction* (New York: Academic Press)
Biryukov A S and Shcheglov V A 1981 *Sov. J. Quantum Electron. (Engl. Transl.)* **11** 1450
Biryukov A S, Serikov R I, Starik A M and Shcheglov V A 1984 *Sov. J. Quantum Electron. (Engl. Transl.)* **14** 575
Cassady P E 1980 *J. Energy* **4** 145
Chakravarty P and Reddy N M 1986 *Appl. Phys. Lett.* **48** 263
Chakravarty P, Reddy N M and Reddy K P J 1987 *AIAA J.* **25** 713
Chakravarty P 1989 *Analysis of two-dimensional downstream-mixing* 16-μm CO_2 *gasdynamic laser* (Ph.D Thesis), Indian Institute of Science, Bangalore, India
Gross R W F and Bott J F 1976 *Handbook of chemical lasers* (New York: John Wiley and Sons)
Losev S A 1981 *Gasdynamic laser*, Springer Series in Chemical Physics, (Berlin: Springer-Verlag) Vol. 12
Manuccia T J, Stregack J A, Harries N W and Wexler B L 1976 *Appl. Phys. Lett.* **29** 360
Munjee S A 1972 *Phys. Fluids* **15** 506; Erratum 1973 *Phys. Fluids* **16** 160
Murthy S N B 1975 *High-power gas lasers*, Inst. Phys. Conf. Ser. (London) No. **29** 222
Saito S, Obara M and Fujioka T 1982 *J. Appl. Phys.* **53** 4616
Wexler B L, Manuccia T J and Waynant R W 1977 *Appl. Phys. Lett.* **31** 730
Wexler B L and Waynant R W 1979 *Appl. Phys. Lett.* **34** 674
Zaroslov D Yu, Islamov R Sh, Karlov N V, Kovalev I O, Konev Yu B, Kuz'min G P and Prokhorov A M 1982 *Sov. J. Quantum Electron. (Engl. Transl.)* **12** 1107